NPL

NPL REPORT ENG 55

Advances in sampling techniques for surface topography measurement – a review

J Wang, R K Leach, X Jiang

SEPTEMBER 2014

Advances in sampling techniques for surface topography measurement – a review

Jian Wang[1,2], Richard K Leach[1,3], Xiangqian Jiang[2]
[1]Engineering Measurement Division, NPL
[2]EPSRC Centre for Innovative Manufacturing in Advanced Metrology, University of Huddersfield
[3]Current address: Department of Mechanical, Materials and Manufacturing Engineering, University of Nottingham

ISSN 1754-2987

National Physical Laboratory
Hampton Road, Teddington, Middlesex, TW11 0LW

Approved on behalf of NPLML by Dr Andrew Lewis, Science Area Leader, Dimensional Metrology

CONTENTS

LIST OF FIGURES

LIST OF TABLES

EXECUTIVE SUMMARY

This report follows on from the PhD research [64] undertaken by the first author and includes an updated review of sampling techniques in the field of surface topography measurement, in particular advances in compressed sensing and scanning techniques.

The output of this review suggests two research directions. First, advanced scanning techniques can be applied at a video-rate to current commercial stylus instruments or probing microscopes for fast measurement. In this case, the Lissajous scan is a highly recommended method for its single frequency input for *x*- and *y*-motion which reduces potential resonances. A stable and high-accuracy mapping algorithm needs to be investigated to map the uneven samples from irregular scan trajectories to a regular grid or some other "intelligent" pattern.

Second, compressed sensing (CS) is a promising solution proposed recently to resolve under-determined measurement systems for sparse signals. Surfaces with high dynamic range (HDR) topography normally have relatively large effective areas and small surface features, which require huge numbers of data points (millions or more) for a full characterisation. However, an efficient measurement can be achieved by relying on the mathematical compressibility of these topographies. Two main problems exist in the application of CS techniques. The first is to find an optimal sparsifying space in which general surface source signals can be concisely expressed. The second is to find stable and highly accurate reconstruction algorithms with fast convergence rates. To the authors' knowledge, CS has not been applied for topography measurement.

1 OVERVIEW OF REPORTED WORK

Sampling is an inevitable step in modern signal measurement. As the most widely used method at present, uniform sampling methods have been widely known for a lack of efficiency for the measurement of high dynamic range (HDR) surfaces [43], which require a regularly high-density but usually redundant sample set to recover the original continuous surface. The HDR surface examples include diverse structured surfaces in optics, micro-fluidics and plastic electronics, which have large effective areas and small embedded geometric features.

Advanced sampling theorems and techniques have been developed during the past decades (see [64]), in particular the last twenty years. Four subdivisions of these sampling techniques can normally be classified according to their mathematical fundamentals.

The first division of sampling techniques is based on statistics. Random, quasi-random and diverse low-discrepancy sampling patterns are in this category. The sampling designs optimise the sampling positions by giving better statistical estimations of the population mean or total related parameters, such as the surface mean roughness, *Sa*.

The second division is based on approximation theories which optimise the sample positions based on a given surface geometric model or earlier samples. The approximation-optimised sampling methods design sample positions by aiming to reduce the approximation error of the substitute geometry constructed from the samples to a source model, using different optimisation algorithms, for example a greedy algorithm [65]. Many model-based sampling and adaptive sampling techniques are in this category.

The third division is the non-uniform sampling techniques developed for the measurement of shift-invariant space signals. The non-uniform sampling techniques claim that an exact recovery of a shift-invariant space signal can be achieved by applying a non-uniform sample design. However, the maximum neighbouring sample distance in these techniques cannot usually exceed half (or other

constants) of the shifting interval of the source signal [3], which implies the required number of sample points would be still large compared to uniform sampling.

The last division includes the compressed sensing (CS)-based sampling techniques. The recent development of CS theorems claims that an exact recovery of a compressible signal can be achieved via an incomplete (less than the Nyquist rate) sampling with a high probability. A larger number of samples means that a recovery with higher accuracy can be made. The advantage of CS techniques stems from the compressibility of the source signal in a specific domain, for example in the frequency domain, scale-frequency domain, or other inner-product domains.

In addition to the main four divisions of sampling techniques, developments in scanning techniques for scanning probe-based instruments have progressed recently. Typical advanced scanning methods include the Lissajous scan, spiral scan and cycloid scan. These methods apply an extremely narrow frequency-band driving signal to avoid exciting the resonance of the instrument by which a video-rate (over 60 frames per second) measurement can be realised.

The findings of this literature review suggest approximation-optimised sampling methods, compressed sensing and anti-resonance scans as the directions for future development. Approximation-optimised sampling can be applied to reduce the number of sampling points for current stylus and scanning-probe-based instruments. CS in topography measurement is in an initial stage of development at the moment, but has high potential. Anti-resonance scans can immediately be applied to current probing instruments for high-speed measurements.

1.1 AGREED SCOPE AND OBJECTIVES FOR THE REVIEW

The scope of the review work is to summarise the advancing trends in the development of sampling techniques which can be applicable to HDR topography measurement. According to the mathematical fundamentals, sampling methods are classified and separately reviewed. Simulations of some mature methods are presented to highlight salient points about the techniques.

1.2 REPORT STRUCTURE

Section 2 constitutes the main review work which includes seven sections. The first three sections sequentially review uniform sampling with Shannon's sampling theorem (in Paley-Wiener space), statistically optimised sampling and approximation-optimised sampling. Next, a section regarding the performance validation for the three previously mentioned methods is given. Section 2.5 reviews advances in the theory of non-uniform sampling of shift-invariant space signals, and in Section 2.6 advances in the theory of sampling of compressible signals are reviewed. Simple numerical cases are given in the latter two sections. The final section gives a review of recently-developed scanning techniques for high-speed measurement. Section 3 presents the conclusions of the review and suggestions for the future research.

2 AN UPDATED REVIEW OF SAMPLING AND SCANNING TECHNIQUES

2.1 UNIFORM SAMPLING AND SHANNON'S THEOREM

A generalised Shannon's sampling theorem normally concerns the recovery of signals in a Paley-Wiener space P_W - a subspace of $L^2(\mathbb{R}^d)$, which contains all the band-limited functions in $B(-W,W)^d$, *i.e.* $P_W = L^2(\mathbb{R}^d) \cap B(-W,W)^d$, in d dimensions [63]. The sampling theorem in a Paley-Wiener space was first formulated by Shannon in 1949 [56]. This theorem has different forms,

for example, the form by Whittaker [67]. Shannon stated that: "If a function $f(t)$ contains no frequencies higher than W cps (cycles per second), it is completely determined by giving its ordinates at a series of points spaced $1/2W$ seconds apart." For convenience, substituting ½ for the bandwidth W, a band-limited function $f(x)$ is in the space $P_{1/2} = L^2(\mathbb{R}^d) \cap B\left(-\frac{1}{2},\frac{1}{2}\right)^d$. A uniform sampling set

$$S = \{f(k), k \in \mathbb{Z}\} \tag{2.1}$$

can ensure an exact reconstruction using the reconstruction equation

$$f(x) = \sum_{k\in\mathbb{Z}} f(k)\,\mathrm{sinc}(x-k). \tag{2.2}$$

The function $\mathrm{sinc}(\cdot - k)$ has the orthogonal property

$$\langle \mathrm{sinc}(\cdot - k), \mathrm{sinc}(\cdot - l)\rangle = \int_{\mathbb{R}^d} \mathrm{sinc}(\cdot - k)\,\overline{\mathrm{sinc}(\cdot - l)}\,dx = \delta(k-l), \tag{2.3}$$

where $\delta(k-l) = \begin{cases} 1, \text{ if } l = k; \\ 0, \text{ if } l \neq k. \end{cases}$ and the bar denotes the complex conjugate (here the conjugate is the sinc function itself).

Shannon's theorem is known to be over-idealised for practical use because:

1) practical signals are never band-limited [58];
2) practical sampling may not be exactly regular due to missing data, disturbance of sampling positions or non-regular sampling designs [8]; and
3) the basis functions $\mathrm{sinc}(\cdot - k)$ have infinite support which is difficult to treat in numerical computation [50].

The traditional three-step sampling techniques, *i.e.* pre-filtering (low-pass filtering is applied to the original signal to force it to be band-limited), sampling and post-filtering (*i.e.* reconstruction), guarantees the input function $f(x)$ is band-limited before sampling. Hence, Shannon's theorem can be applied to the three-step sampling techniques. In the measurement of surface topography, the employed mechanical or optical probes produce a pre-filtering of the real surface, which has been demonstrated to be traceable and stable with proper calibration processes [16, 41]. However, the issues regarding the non-regularity of practical sampling patterns and the infinite support of the recovery basis function are still troublesome. For example, if applying a truncation of the reconstruction sinc function, a ringing effect in the frequency domain can be excited [50, 54].

However, uniform sampling is the most popular method in the design of current measuring instruments. The advantages of uniform sampling include the easily understandable and robust theoretical basis in sampling and time series-related computations, for example, the fast Fourier transform (FFT), cross-correlation and convolution. The advantages of uniform sampling methods are usually preferred compared to the three over-idealised issues discussed previously.

2.2 STATISTICALLY OPTIMISED SAMPLING

2.2.1 Jittered uniform sampling

Shannon's theorem indicates that a signal with infinite frequency spectrum cannot be exactly reconstructed by a uniform sampling sequence due to the existence of unavoidable spectral aliasing.

However, the sampling error due to aliasing can be reduced by varying the spacing between the sample positions in a non-uniform way [52].

Random sampling has been suggested as one of the most optimised sampling methods due to its capability for an unbiased estimation and the characteristic of anti-spectral aliasing. Jittered uniform sampling is a variation of random sampling which combines a uniformly defined pre-stratification and a random allocation of sample points within each stratified area. Random sampling methods can convert aliased frequency components into noise. For example in Figure 2-1, an uniform sampling presents zig-zag distortions for the far end area of the checkerboard, while jittered uniform sampling converts the coherent distortions into noise which can be more statistically stable.

Let $X_U = \{x_j : j \in J^d\}$ be a uniform sampling set, where J^d is a countable index set in *d*-dimensions, *i.e.* $\forall j, j-1 \in J$, $x_j - x_{j-1} = T$, where T is the sampling period $T \in \mathbb{R}^d$. Then let Y be a random jittering disturbance sequence, *i.e.*

$$Y = \left\{ y_j : y_j \in \left(-\frac{\Delta}{2}, \frac{\Delta}{2}\right), \Delta \le T, j \in J^d \right\}. \tag{2.4}$$

A jittered uniform sampling set can be generated by

$$X_{\text{Jittered}} = \{ z_j : z_j = x_j + y_j, x_j \in X_U, y_j \in Y \}. \tag{2.5}$$

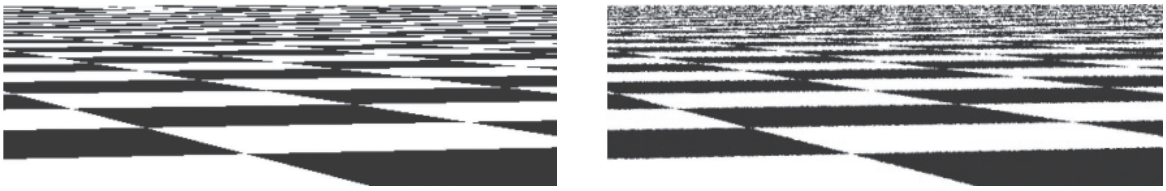

(a) (b)

Figure 2-1. The spectral aliasing effect in (a) uniform sampling and in (b) jittered uniform sampling [52].

2.2.2 Low-discrepancy patterns

Another statistically optimised sampling is the so-called low-discrepancy sampling. Low-discrepancy sampling optimises the sampling positions to minimise the evaluation discrepancies between the means or sum totals of the sample, and the population. Low-discrepancy sampling predicates that smaller sample sets with a specially designed pattern can produce higher reconstruction accuracies than uniform sampling.

To evaluate the discrepancy of a sample set, the basic procedure is to evaluate the volume of a box b which belongs to $B = [0,u]^n : u \in (0,1)$, by placing points $X_P = \{x_i \in [0,1]^n : i \in 1,2,...,N\}$ in a specific form P (such as the uniform form) into the domain $[0,1]^n$, and calculating the ratio of the number of points inside b over the total number, *i.e.* $\#(X_P \bigcap b)/N$. It can be known [52] that $\#(X_P \bigcap b)/N$ is an approximation to the volume of the box b given the sample points X_P, *i.e.*

$$\mathrm{E}(\#(X_P \bigcap b)/N) = V(b), \tag{2.6}$$

where $V(b)$ is the volume of region b. An illustration of this approximation idea is shown in Figure 2-2 in which b has the size 0.12. Thus the discrepancy of the finite sampling X_P to approximate the area of region b can be defined as

$$D_N(B, X_P) = \sup_{b \in B} \left| \frac{\#(X_P \cap b)}{N} - V(b) \right| \tag{2.7}$$

where "sup" denotes the supremum of a set.

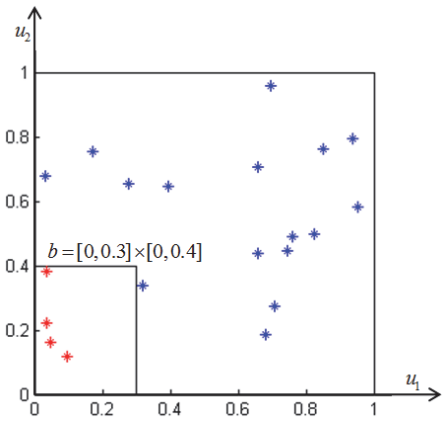

Figure 2-2. Illustration of approximation of the area of the square *b*.

The distribution pattern of the sample points P determines the magnitude of the discrepancy D. Therefore, there are optimised sampling sequences or patterns which can limit the evaluation discrepancy within a proper range. For example, let X_P be a uniform sampling set in one-dimension, *i.e.*, $X_P = (i/N, i = 1,2,...,N)$, and b be a box $b = [0,1/N)$ which has the volume $V(b) = 1/N$. Then $D_N = 1/N$ can be obtained because $\#(X_P \cap b) = 0$. However, if $X_p = \frac{i-1/2}{N}, i = 1,2,\dots,N$, then $D_N = 1/2N$. Many researchers have contributed to this statistical problem [55, 68].

Considering a one-dimensional case, one of the simplest low-discrepancy sequences is the van der Corput sequence [62], which is given by the radical inverse function $\Phi_b(i)$ in base $b = 2$, *i.e.*

$$X = \{x_j : x_j = \Phi_2(j) = 0.d_1 d_2 \dots d_m, j \in J\}, \tag{2.8}$$

where d_i satisfies $\sum_{i=1}^{+\infty} d_i b^{i-1} = j$ in base $b = 2$. For instance, the first ten points in the sequence are $\left\{\frac{1}{2}, \frac{1}{4}, \frac{3}{4}, \frac{1}{8}, \frac{5}{8}, \frac{3}{8}, \frac{7}{8}, \frac{1}{16}, \frac{15}{16}, \frac{5}{16}\right\}$. The first ten points of the van der Corput sequence in base 3 are $\left\{\frac{1}{3}, \frac{2}{3}, \frac{1}{9}, \frac{4}{9}, \frac{7}{9}, \frac{2}{9}, \frac{5}{9}, \frac{8}{9}, \frac{1}{27}, \frac{10}{27}\right\}$. The intelligent sequence has the discrepancy

$$D_N(X) = O(\log N / N). \tag{2.9}$$

Based on the van der Corput sequence, two well-known low-discrepancy sequences that are defined in an arbitrary number of dimensions are the Halton [30] and Hammersley [31] sequences. The two patterns are separately defined as follows:

$$X_{Ham} = \left\{x_j : x_j = \left[\frac{j}{N}, \Phi_{b_1}(j), \Phi_{b_2}(j), \ldots, \Phi_{b_{d-1}}(j)\right], j \in J\right\}, \tag{2.10}$$

$$X_{Hal} = \left\{x_j : x_j = \left[\Phi_{b_1}(j), \Phi_{b_2}(j), \ldots, \Phi_{b_d}(j)\right], j \in J\right\}, \tag{2.11}$$

where b_i are the relative primes. Usually b_i can be set as the first $d-1$ or d primes in $\mathbb{Z}^+$, such as 2, 3, 5, 7 and so on. If $d = 2$, the first 100 points of the Hammersley and Halton sequences are shown in Figure 2-3.

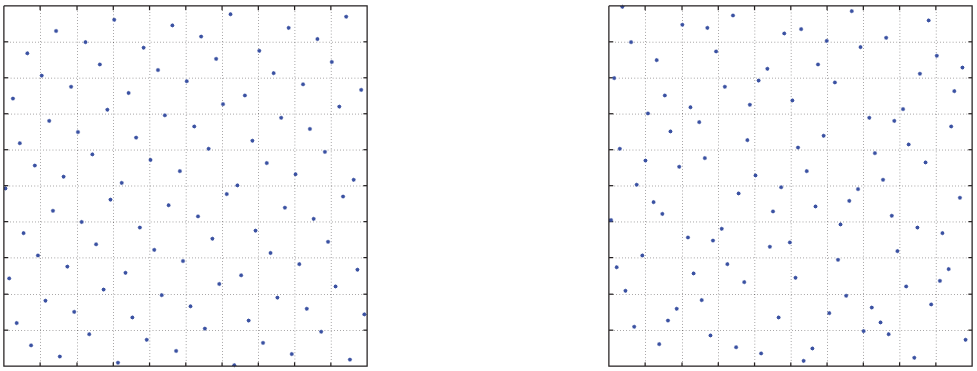

(a) A Hammersley pattern (b) A Halton pattern

Figure 2-3. The 100-points sampling patterns of Hammersley and Halton sequences.

In addition to the two classical sequences, there are many other variations such as the Sobol sequence, Hammersley-Zaremba, Halton-Zaremba and [t,s] sequences. A computational investigation of the diverse techniques can be found elsewhere [38].

In surface metrology, low-discrepancy sampling techniques were initially introduced in [68] where the Hammersley sequence and Halton-Zaremba sequence were used to calculate the surface roughness and flatness of planar surfaces. Later, in [44], the root mean square errors (RMSEs) of the selected indicators, for example surface roughness *Sq*, were estimated for different simulated surfaces. All these results show that a low-discrepancy sampling sequence is more effective than random or uniform sampling methods, in terms of the improvement of measurement accuracy or reduction in the number of sample points. In 2000, Kim [37] analysed the RMS deviations and efficiency of low-discrepancy sampling methods in flatness measurement using CMMs. It can be found that for practical measurement, the improvement in accuracy of low-discrepancy sampling methods is not clear compared to uniform sampling.

In one of the authors' simulations [66], no convincing evidence was found to demonstrate the efficiency of the Halton and Hammersley patterns. For example, Figure 2-4 and Figure 2-5 show the performance of uniform sampling, jittered uniform sampling, Hammersley pattern and Halton pattern for the measurement of the surface root mean square (RMS) roughness, extreme height and RMS height deviations for stochastic and HDR topographies respectively. In each test, one hundred simulations were carried out and the indicators were shown with their means and variation ranges (the vertical bars in Figure 2-4 and Figure 2-5). The results do not consistently show unsatisfying performance for uniform sampling methods. This finding contradicts that of former researchers' results [44, 68], which needs further research.

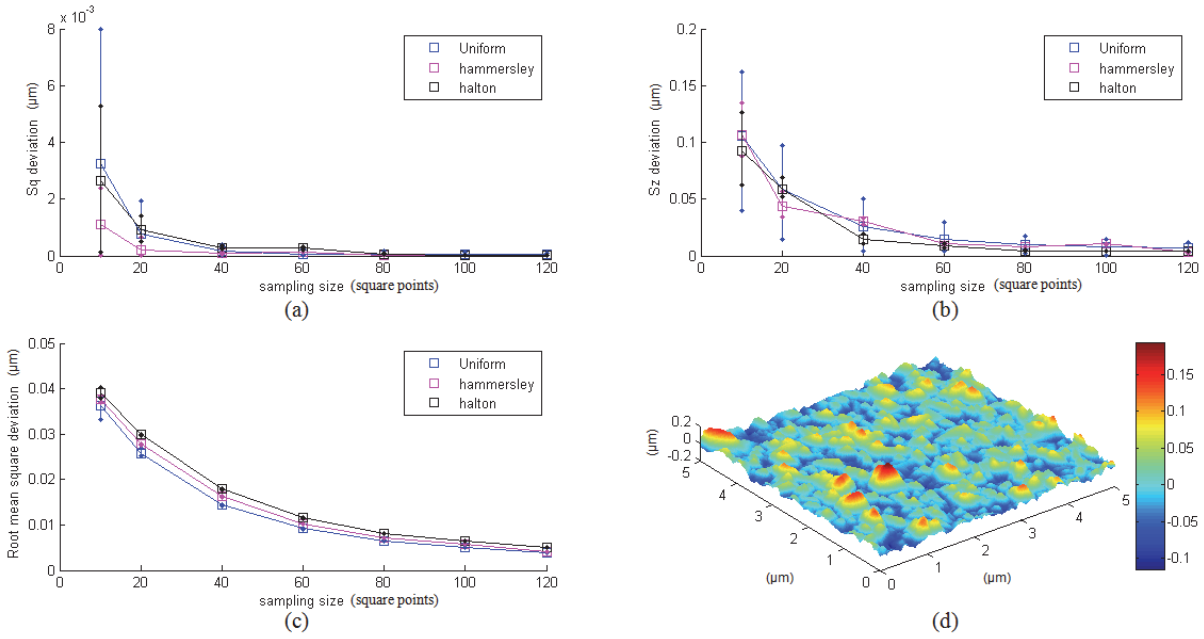

Figure 2-4. Comparison of uniform, Hammersley and Halton sampling for the measurement of a normal EDM surface, by estimating (a) Sq, (b) Sz and (c) root mean square deviation from (d) the original data (512 × 512 points).

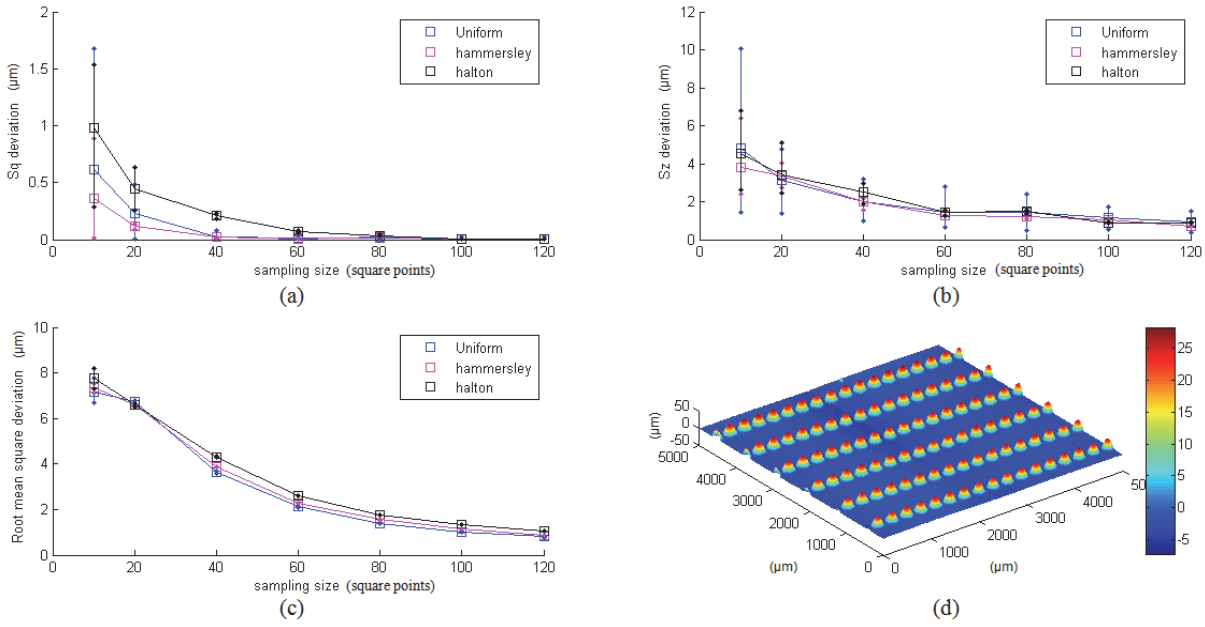

Figure 2-5. Comparison of uniform, Hammersley and Halton sampling for the measurement of a micro-lens array, by estimating (a) Sq, (b) Sz and (c) root mean square deviation from (d) the original structured data (800 × 800 points).

2.3 APPROXIMATION OPTIMISED SAMPLING

Since an exact recovery of real world signals is usually impossible, metrologists work on providing sampling solutions to approximate the source signal to within an acceptable accuracy. Much work has been carried out to achieve this objective.

In coordinate metrology and surface metrology, researchers tend to enhance measuring efficiency using adaptive or model-based (adaptive) sampling. Adaptive sampling uses iterative searching methods on an error space which determines new sampling positions based on earlier sample results [5, 23]. Model-based sampling uses a given population model (for example, a CAD model or a probability distribution function) [24, 57] to design the sample at key positions which contributes highly to the recovery accuracy. For example, with an initial sampling set, a substitute geometry of the source surface can be approximated. By comparing the substitute geometry with the original geometry, the positions with higher deviations can be found and new samples are added in these areas to minimise the evaluation error in the next iterative loop. Diverse adaptive sampling and model-based sampling designs have been developed based on different approximation methods during the last twenty years [5, 23-25, 40, 44, 51, 52, 57, 65, 68].

2.3.1 Model-based sampling

Cho and Kim [15] developed an adaptive sampling method based on a mean-curvature analysis and different probe path generation algorithms were tested. Killmaier *et al.* [36] presented a solution for the measurement of a workpiece which detects the standard geometric features, such as straight lines, circles, columns, cones or peaks, by using a genetic algorithm, and then the distribution of sampling points is allocated by establishing a knowledge-based system. Elkott introduced several CAD-based sampling methods for freeform surface metrology, which include four kinds of automatic sampling methods [24], a curvature change-based sampling method and an iso-parametric sampling method [25]. Shih *et al*. [57] developed three kinds of adaptive sampling methods for coordinate metrology, including the so-called direct sampling, indirect sampling and local adjustment sampling methods. Recently, discrete wavelet decomposition-based adaptive sampling techniques have also been proposed [51]. More published work is listed in Table 2-1 in chronological order.

Table 2-1. A comparison of existing model-based sampling designs.

Year	Authors	Contributions	Characteristics	Applications
1991	Terzopoulos *et al.* [60]	Adaptive mesh sampling based on a 'node-spring system' on an initial regular mesh where regions with high gradient are sampled densely	iterative, bilinear interpolation	computer graphics
1995	Tanaka [59]	Iteratively triangularises surface hierarchically into triangle patches according to local surface properties such as orientation, curvature and colour (or height)	iterative, triangularisation	computer graphics
1995	Li 1995 [45]	A simple iterative mesh generation based on surface curvedness where regions with high curvedness are sampled densely	iterative, curvedness, bilinear interpolation	computer graphics, CAD
1995	Cho *et al.* [15]	Ranks a series of sub-regions by mean curvatures, and then allocates new sampling points in selected regions iteratively	iterative, surface curvature ranking	CMM measurement

2002	Elkott *et al.* [24]	Proposes four adaptive sampling methods for NURBS models based on patch size or Gaussian curvedness, etc.	NURBS models, patch properties ranking, non-iterative	CMM measurement
2003	Killmaier *et al.* [36]	Detects standard geometrical primitives using genetic algorithm, and aims to give an optimal number and distribution of sampling points	genetic algorithm, knowledge-based system	CMM measurement
2005	Elkott *et al.* [25]	Proposes three adaptive sampling methods based on iso-parametric lines of NURBS models: automatic sampling, curvature-change based sampling, and iso-planar sampling	NURBS models, non-iterative and iterative	CMM measurement
2006	Petkovski [51]	A discrete wavelet transform (DWT)-based adaptive sampling algorithm which is essentially equivalent to curvature analysis	DWT analysis, patch properties ranking, non-iterative	Signal processing
2008	Shih *et al.* [57]	Proposes three adaptive sampling methods: direct sampling (quadtree hierarchical division), indirect (two-dimensional binary tree hierarchical division) sampling and local adjustment	iterative, root mean square error evaluation, local adjustment	CMM measurement, CAD

Summaries of approximation model-based sampling can be given based on the previous developments.

1. Most (not all) model-based sampling methods adopt an iterative algorithm to optimise the sample positions. The final sampling result is sensitive to the initial conditions, for example the initial sample positions, in the execution of the algorithms [23]. Model-based sampling methods can easily adapt sampling designs to a pre-defined accuracy.
2. The concept of hierarchical stratifying of a surface population prevails in much sampling design work [15, 51, 59]. With a hierarchical stratification, a surface can be subsequently divided into strata of areas with different surface complexities, for example local mean curvature or local mean approximation deviation. For higher strata, dense sampling points are allocated; while for low strata, sample points are sparse. An advantage of the hierarchical stratification is that the sampling points can be locally regular. Therefore, the local uniform sample designs can easily be executed using current surface measuring instruments.
3. Model-based sampling methods have difficulties in practical measurement due to the lack of consideration of unexpected defects of a practical workpiece. It is also difficult to control the positioning error when matching the computationally designed sample positions to a real surface product.
4. For many model-based sampling methods, a rough preliminary measurement can be used as a substitute of the surface model. In this way, the model-based method can be used in most practical measurements in which a CAD model is unavailable.
5. If a preliminary measurement is given with a dense sample setting, model-based sampling methods provide an adaptive compression of the samples at a specific accuracy. Such compressions are useful in data storage and other applications, for example providing fiducial marks for the registration of two sets of point cloud.

Overall, model-based methods can be of potential use in surface measurement. If the CAD model is substituted by a preliminary measurement, a general-purpose efficient measurement device can be easily constructed.

2.3.2 Adaptive sampling

Non-model-based adaptive sampling methods have the ability to adjust their sampling points in real time. For example, Edgeworth and Wilhem [23] proposed a real-time adaptive sampling method based on the earlier sampling results by analysing the surface normal. Hu *et al.* [32] proposed an adaptive scanning strategy, which automatically adjusts its sample step length, by estimating surface slope variations using extrapolation. The authors developed an adaptive sampling method called sequential profiling adaptive sampling [65], which has been demonstrated to give a 40 % to 60 % reduction in the required number of sample points. The sequential profiling adaptive sampling method can easily be applied to the current scanning instruments.

Different from model-based sampling, adaptive sampling methods can avoid the inherent positioning errors of the model-based methods and are able to effectively pick up the necessary information to identify unexpected defects. Adaptive sampling is a real-time sample-designing method, which indicates that the design may not be globally optimised as with model-based sampling methods. The sampling results are generally sensitive to the initial conditions, such as the initial sample positions. However, adaptive sampling methods can easily generate good sampling results without an accurate pre-positioning of a real surface.

Currently, many adaptive sampling methods have been developed for coordinate measurement systems. These adaptive sampling methods can be applied to surface topography measurements using scanning surface instruments with proper consideration for the differences in the scanning mechanisms. For example, scanning instruments use fast raster scans as the scanning method which have differing positioning accuracy when the scanning is along the *y*-direction compared to the *x*-direction.

2.4 PERFORMANCE VALIDATION AND DISCUSSION

A performance test of several selected intelligent sampling methods has been carried out [64, 66]. The seven tested sampling methods include uniform sampling, jittered uniform sampling, Hammersley pattern sampling, Halton pattern sampling, rectangular subdivision adaptive sampling, triangle subdivision adaptive sampling and sequential profiling adaptive sampling [66]. The advantages of the approximation-optimised sampling methods, *i.e.* the tested three adaptive sampling methods, are prominent compared to uniform sampling and statistically optimised methods.

Table 2-2 shows the different evaluation indicators for the seven selected sampling methods, which were tested on three structured surfaces: a linear pattern, a tessellation pattern and a rotational symmetric pattern (see [66] for a graphical view). The three graphs in the first row of Table 2-2 show the RMS height deviations of the sampling-reconstructed surface from the ‘standard’ measurement results. The second row shows the evaluation errors of the key feature attributes for the three specimens, including respectively the groove width for linear pattern, the pitch distance for tessellation and the radius for the rotational symmetric pattern. The third row presents the evaluation errors of step heights for the linear and the tessellation patterned specimen, and the roundness of the boundary for the central lens of Specimen 3. Most of the evaluation indicators decrease in the form of a power function versus the number of sample points. Therefore, the evaluation data were fitted using power functions and all the graphs in Table 2-2 were shown in log-log forms. A few exceptions of the decreasing performance happen such as in Table 2-2(h) where the triangle and rectangle subdivision adaptive sampling methods perform worse when sample points increase. The exceptions may originate

from the limited data points for fitting. For example, due to the fact that the circle boundary recognition fails, there are only three valid indicator points in the test of rectangle subdivision adaptive sampling method.

Table 2-2. Deviations of the evaluation parameters from the standard result for different specimens. (log-log plots)

Specimen 1: Linear patterned topography

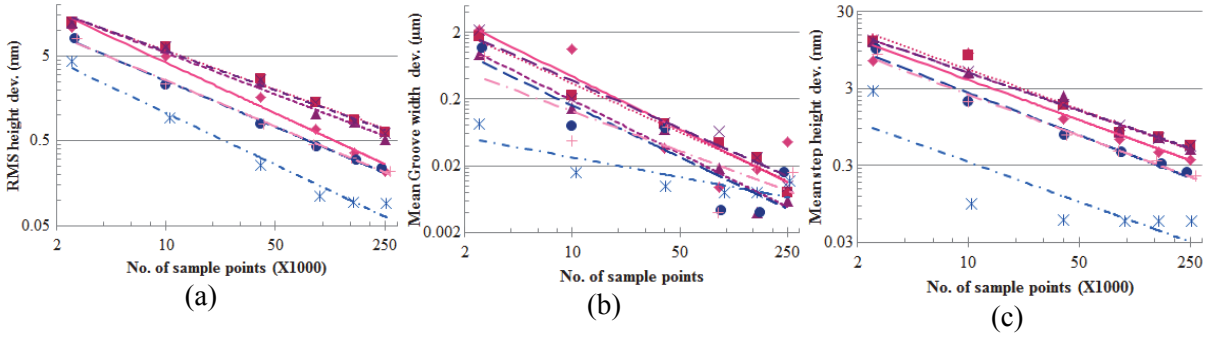

Specimen 2: Crossed grating topography

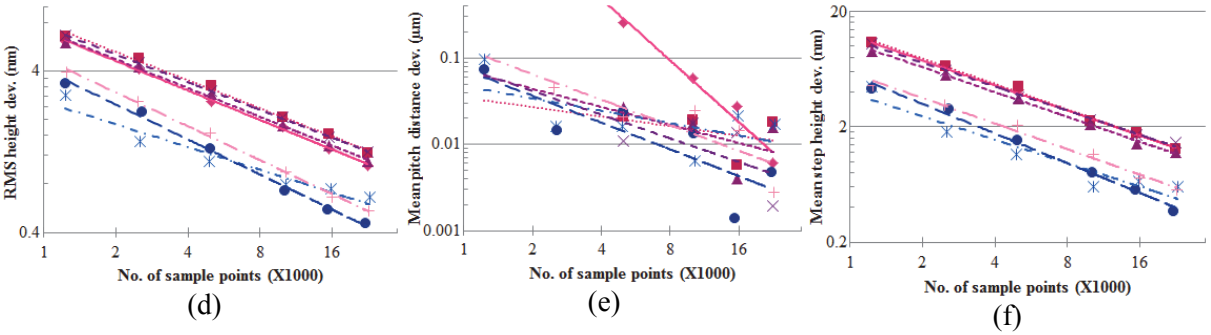

Specimen 3: Fresnel lens topography

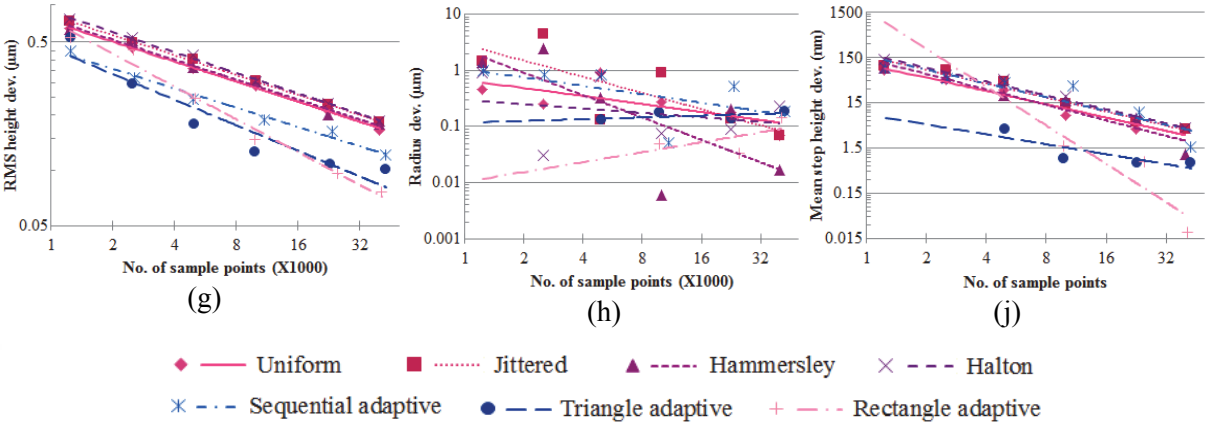

It can be seen from Table 2-2 that the low-discrepancy pattern sampling methods have similar performance to uniform or jittered uniform sampling. For the measurement of structured surfaces, the advantages of low-discrepancy pattern sampling are not apparent and sometimes these methods may not perform better than uniform methods. In some situations, uniform sampling may be a better solution compared to other fixed patterns.

The advantages of approximation optimised sampling methods are appreciable. These methods allocate the sampling effort according to their earlier sample results or given models. In other words,

they can adapt the sampling effort to key positions, which have higher impact factors on enhancing the reconstruction accuracy than others. Although adaptive sampling methods have no clear advantages on measuring the pitch distance of crossed-gratings (see Table 2-2e), they have been shown to be effective in the measurement of other structured surfaces and with other parameters.

There are challenges, however, to applying approximation optimised sampling to practical measurement. Sequential profiling adaptive sampling may suffer from the mechanical constraints of stability (for example, thermal drift) and accuracy in the *y*-direction scanning. Most of the other approximation optimised sampling methods are difficult to implement within the operation envelope of scanning instruments, regarding the complex scan route designs and redundant scan durations. In terms of interferometers, many of the reviewed sampling methods may be promising, with the assistance of a high resolution CCD and pixel stratification, or lens auto-switch systems. Considering the unavoidable positioning errors in the installation of the specimens and optical resolution constraints, specialised research work on intelligent sampling for interferometers may be required. In addition, more theoretical work is necessary to further the research on intelligent sampling. For example, non-regular sample data storage solutions need to be reconsidered contrary to the current grid data storage. The reverse problem of sampling and reconstruction needs to be fully investigated for the applications of geometric measurement. Also, determination of the sample size for a sampling strategy is a complex problem which requires further attention.

2.5 SAMPLING OF SHIFT-INVARIANT SPACE SIGNALS

2.5.1 The theorem

In the sixty years following the development of Shannon's sampling theorem, researchers have tried to extend the theory to avoid its practical limitations, for example the infinite support of the reconstruction filter function and band-limited assumption. A sampling theory in shift-invariant spaces has been systematically demonstrated in the early twenty-first century [3, 8, 29]. The novel theory is a great improvement on the traditional Shannon sampling theorem, which can be applied to non-uniform sampling situations and the applicable functions are no longer a band-limited function in a Paley-Wiener space P_W . The theoretical completeness of this theory has been demonstrated from mathematics [3]. However, the numerical operation in practice still has some difficulties. Extensive knowledge of function analysis, frame theory, wavelet theory and signal processing is necessary to fully understand the shift-invariant space sampling theorem, which limits its wide application in engineering. Here, an outline introduction to the theorem is given.

Given a generator $\varphi(x)$, a shift-invariant space [1, 3] is defined as

$$V_v^p(\varphi) = \left\{\sum_{k\in\mathbb{Z}^d} c_k \varphi(\cdot - k) : c \in l_v^p\right\}, \tag{2.12}$$

where φ is a generator function, which can be a wavelet, spline basis function or other function, v is a non-negative weighting function, p defines a p-norm, which implies that $c \in l_v^p$, *i.e.*

$$\|c\|_{l_v^p} = \|cv\|_{l^p} = \sum_{k\in\mathbb{Z}^d} |c_k|^p v(k)^p < +\infty. \tag{2.13}$$

It follows that if v=1 , p=2, and φ=sinc(·) , the shift-invariant space is a Paley-Wiener space [63] and Shannon's theorem applies. This generated function space is known as translationally invariant, *i.e.* if $f \in V_v^p$, then $f(\cdot - y) \in V_v^p$. It is apparent that the shift invariant space covers far more signals in practice compared to P_W .

The sampling theory in shift invariant space [3] includes numerous propositions which can be summarised in the following:

1. If $\varphi \in W_0(L_v^1)$ (many basis functions belong to this space, for example a second or higher order B-spline basis[1] [2, 46, 63]), *i.e.* φ is a continuous function (order zero) in a Wiener amalgam space $W(L_v^1)$ for which

$$W\left(L_v^p\right) = \{f: \sum_{k\in\mathbb{Z}^d} \text{esssup}\{|f(x+k)|^p v(k)^p : x \in [0,1]^d\} < \infty\}, \tag{2.14}$$

$V^2(\varphi)$, *i.e.* V_v^p with $v = 1$ and $p = 2$, is a reproducing kernel Hilbert space (RKHS) [71], and the kernel functions can be obtained by

$$K_x(y) = \sum_{k\in\mathbb{Z}^d} \overline{\varphi(x-k)}\tilde{\varphi}(y-k), \tag{2.15}$$

such that $f(x) = \langle f, K_x \rangle$, where $\tilde{\varphi}$ is a unique dual generator of φ which satisfies

$$\langle \tilde{\varphi}(\cdot), \varphi(\cdot - k) \rangle = \delta(k)^2. \tag{2.16}$$

2. Given a separated[3] sampling set $X = \{x_j, j \in J\}$ of $f \in V^2(\varphi)$, where J is a countable indexing set, the reproducing kernel function sequence $\{K_{x_j}, x_j \in X\}$ constructs a frame [22] for $V^2(\varphi)$ (*i.e.* $\{K_{x_j}, x_j \in X\}$ and is a Reisz basis of $V^2(\varphi)$) if and only if X is a stable sampling set, *i.e.*

$$f(x) = \sum_{j\in J} \langle f, K_{x_j} \rangle \widetilde{K}_{x_j} = \sum_{j\in J} f(x_j)\widetilde{K}_{x_j}, \tag{2.17}$$

where $\{\widetilde{K}_{x_j}, x_j \in X\}$ is a dual frame of $\{K_{x_j}, x_j \in X\}$, according to the frame theory [22].

In other words, a f in $V^2(\varphi)$ can be exactly recovered from a stable sampling set $X = \{x_j, j \in J\}$ if and only if $\{K_{x_j}, x_j \in X\}$ is a Riesz basis.

However, the dual frame $\{\widetilde{K}_{x_j}, x_j \in X\}$ is very difficult to find in practice; iterative algorithms are suggested.

3. Let $\varphi \in W_0(L_v^1)$, P be a bounded projection from L_v^p to V_v^p, for example,

$$\text{P}: f \to \sum_{k\in\mathbb{Z}^d} \langle f, \tilde{\varphi}(.-k) \rangle \varphi(\cdot - k), \tag{2.18}$$

and let Q_X be a quasi-interpolant based on a sample set $X = \{x_j, j \in J\}$, which has

---

[1] A B-spline basis with order N has the form $\beta_N = \chi\left[-\frac{1}{2},\frac{1}{2}\right] * \chi\left[-\frac{1}{2},\frac{1}{2}\right] * \ldots * \chi\left[-\frac{1}{2},\frac{1}{2}\right]$ (N-1 times fold convolution of the order 0 basis function).

[2] $\delta(k)$ is a Dirac delta function which has $\delta(0) = 1$ and $\delta(k) = 0$ for $k \neq 0$.

[3] "Separated" here means for $\forall i \in \mathbb{Z}^d$, $x_i \neq x_{i+1}$.

$$\mathrm{Q_X} f = \sum_{j \in J} f(x_j)\beta_j \,, \tag{2.19}$$

where $\{\beta_j\}_{j\in J}$ is a partition of unity (*i.e.* $0 \le \beta_j \le 1$ for $j \in J$; $\operatorname{supp}\beta_j \subset B_\gamma(x_j)$ [4] and $\sum_{j\in J}\beta_j = 1$, for example a B-spline basis [17] in Figure 2-6), then there exists a stable sample set $X = \{x_j, j \in J\}$ with sample density $\gamma > 0$ such that any $f \in V_\nu^p$ can be recovered from the sample by the iterative algorithm

$$\begin{cases} f_1 = \mathrm{PQ_X} f \\ f_{n+1} = \mathrm{PQ_X}(f - f_n) + f_n \end{cases} \quad \text{(see Figure 2-7).} \tag{2.20}$$

The sample density γ satisfies the definition

$$\bigcup_{j\in J} B_\gamma(x_j) = \mathbb{R}^d, \tag{2.21}$$

i.e. the distance of any sample point to its next neighbour is at most 2γ.

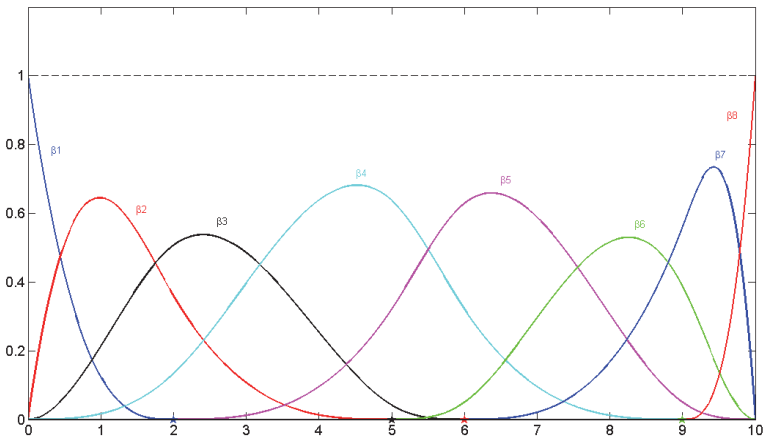

Figure 2-6. A partition of unity with a third degree B-spline basis (knots: 2, 5, 6, 9).

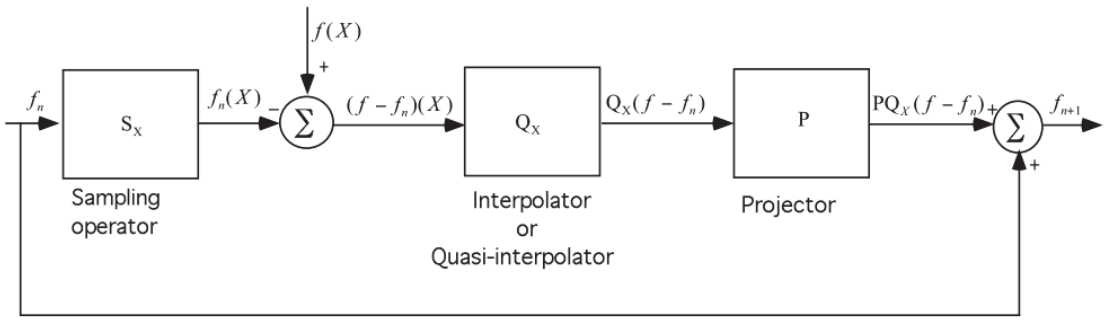

Figure 2-7. The iterative reconstruction algorithm based on equation (2.20) [3].

[4] $B_\gamma(x_j)$ is a continuous bound set $B_\gamma(x_j) = [x_j - \gamma, x_j + \gamma]$.

2.5.2 Numerical studies

Fast local algorithms have been proposed [29] for a small number of sample points. To recover a shift-invariant signal, researchers can simply solve the (infinite) system of linear equations

$$\sum_{j\in J} c_k \varphi(x_j - k) = f(x_j) \tag{2.22}$$

for the coefficients $\{c_k\}$. To be precise, with a finite sample set $X = \{x_1, x_2, ..., x_N\}$ and a finite length signal $f = \sum_{k=1,..K} c_k \varphi(\cdot - k)$, the following matrix is constructed

$$U = \begin{bmatrix} u_{x_1,1} & \cdots & u_{x_1,K} \\ \vdots & u_{x_n,k} & \vdots \\ u_{x_N,1} & \cdots & u_{x_N,K} \end{bmatrix}, \text{ where } u_{x_j,k} = \varphi(x_j - k), \tag{2.23}$$

and $c = [c_1, c_2, ..., c_K]^{\mathrm{T}}$. Thus the linear system to be solved in equation (2.22) can be written in the form

$$Uc = f\big|_X \tag{2.24}$$

where $f\big|_X$ is a vector containing the sample values, which have $f\big|_X = [f(x_1), f(x_2), ..., f(x_N)]^T$. This linear system can be solved easily [28].

A numerical example can be found in Figure 2-8 in which the reconstruction error is calculated as

$$Error = \frac{\left\| f_{rec}\big|_X - f\big|_X \right\|^2}{\left\| f\big|_X \right\|^2}. \tag{2.25}$$

If Gaussian random noise with 0.1 as the standard deviation is added to the sampling process of the signal in Figure 2-9a, the fast local algorithm also works stably and provides an approximation of the noisy samples in $V^2(\varphi)$ (see Figure 2-9). It can be found that if the generator function of the shift-invariant space signal is known, the original signal can be exactly or approximately recovered depending on different noise levels using the local linear method.

In summary, the sampling theorem in shift-invariant spaces extends the Shannon sampling theorem. The shift-invariant space sampling theorem states that a shift-invariant signal can be exactly recovered from a stable sampling set with properly defined sampling density γ. Such a sampling set allows a limited disturbance of the sample positions centred on a uniform grid.

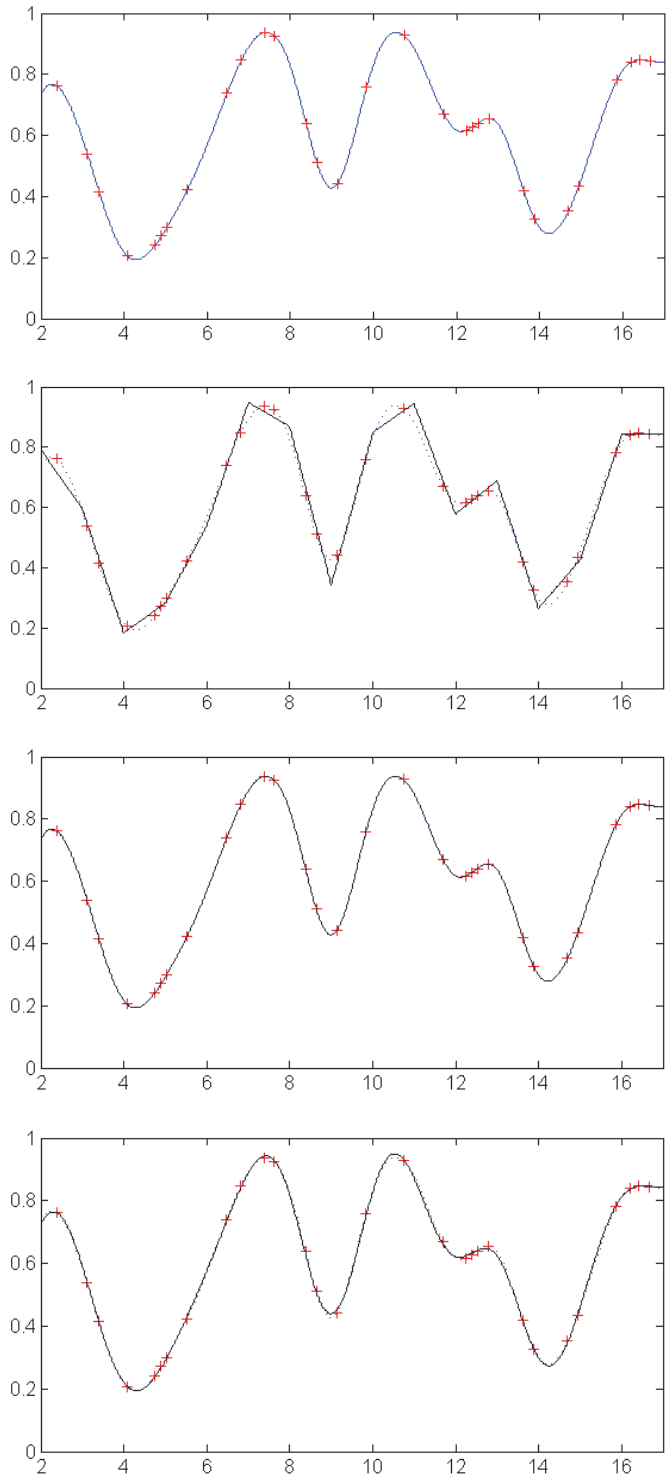

(a) Original signal in third degree B-spline β3 shift-invariant subspace and a set of samples

(b) Reconstruction using the first degree B-spline (error result: 7.1×10^{-4}).

(c) Reconstruction using the third degree B-spline (error result: 1.7×10^{-30}).

(d) Reconstruction using the fifth degree B-spline (error result: 5.9×10^{-5}).

Figure 2-8. Reconstruction of a shift-invariant signal using fast local algorithms. (a) shows the original signal which is generated by the third degree B-spline β_3 (blue curve) and a non-uniform sample set with density $\gamma = 0.5$ (red dots); (b), (c) and (d) show the reconstructed continuous signal using the first, third and fifth degree B-spline respectively (the black curve is the reconstructed signal, the blue dashed curve is the original signal).

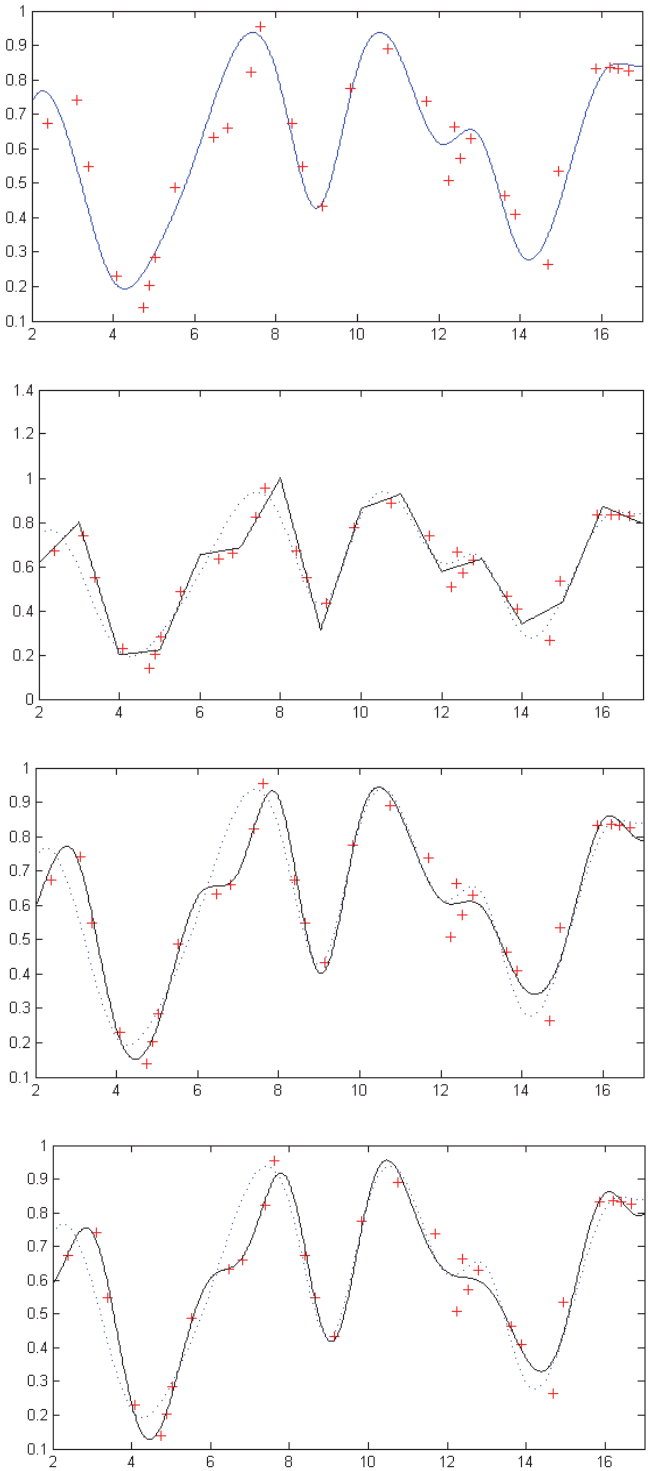

(a) Original signal and noisy samples.

(b) Reconstruction using the first degree B-spline (error result: 12.2 %).

(c) Reconstruction using the third degree B-spline (error result: 11.2 %).

(d) Reconstruction using the fifth degree B-spline (error result: 12.4 %).

Figure 2-9. Reconstruction of a randomly noised shift-invariant signal. (a) shows the original shift invariant signal which is generated by the third degree order B-spline β_3 (blue curve) and a noisy sample set with density $\gamma = 0.5$ (red dots); (b), (c) and (d) show the reconstructed continuous signal using the first, third and fifth degree B-spline respectively (black curve is the reconstructed signal, blue dashed curve is the original signal).

In the measurement of HDR topographies, many signals have different frequency components regionally or have a sparse distribution of the features of interest, which indicates that the structured surface signals may not be able to be efficiently approximated in a shift-invariant space. Rather, it may be valuable to consider such a space for structured surfaces such that

$$V^2(\varphi) = \left\{\sum_{k\in\mathbb{Z}^d} c_k \varphi\,(\cdot - x_k), c \in l_v^p\right\}. \tag{2.26}$$

where $\{x_k\}$ is a separated increasing sequence, *i.e.* $x_k < x_{k+1}$ for $\forall k \in \mathbb{Z}^d$. However, another barrier for such an approximation comes from the unknown distribution of $\{x_k\}$, hence the approximation of HDR topography using (2.26) is difficult to implement in practice.

2.6 SAMPLING OF COMPRESSIBLE SIGNALS

Recently, a new theory, referred to as compressed sensing [10, 20, 47], which detects a signal by sampling at a dramatically reduced rate has drawn wide interests across academia. A successful application of this theory is the single pixel camera developed at Rice University [21]. This technique transforms a scene image into a series of single pixel light intensities using a spatial light modulator (encoding). With over thousands of encoding at random and sensor detections, a mega-pixel image can be recovered at a specific level of accuracy. An introductory note about compressed sensing techniques can be found elsewhere [4].

2.6.1 Incomplete sampling and L1-minimisation recovery

The sub-sampled signal recovery problem can be formulated in the following form. Given a source signal x in vector form of size N, *i.e.* $x \in \mathbb{R}^N$, if taking K linear measurements with a given measuring vector φ_k (for example, a Dirac delta function or the K^{th} row vector of the Fourier transform matrix), the measurements y can normally be expressed as

$$y_k = < x, \varphi_k >, k = 1,2,...,K \text{, or } y = \Phi x, \tag{2.27}$$

where φ_k forms each row of Φ.

If the measurements y are obtained, and given $K << N$, equation (2.27) becomes an underdetermined system to resolve the source signal x. Shannon's theorem indicates that if x has N degrees of freedom, x can only be exactly recovered by $K \geq N$ distinct measurements.

However, if x is S-sparse, *i.e.* x has the support $\{i: x_i \neq 0\}$ of cardinality (size) less or equal to S, and

$$C \cdot S \cdot \log N \leq K, \tag{2.28}$$

given Φ consisting of K rows of discrete Fourier transform (DFT) matrix selected uniformly at random, Candes, Romberg and Tao [12, 13] demonstrated that x can be exactly recovered by solving the following constrained convex problem using an L1-norm minimisation algorithm

$$\text{BP: } \hat{x} = \text{argmin}_{x\in\mathbb{R}^N} \|x\|_{l1}, s.t. \|y - \Phi x\|_{l2} \leq \varepsilon, \tag{2.29}$$

where ε quantifies the uncertainty of noisy measurement y, which can normally be specified in advance for a measurement. According to the compressed sensing theorems, x can be recovered at a high probability if the measurement matrix Φ obeys a uniform uncertainty principle (UUP) [12].

The optimisation problem in equation (2.29) is also regarded as the Basis Pursuit, in which (2.29) can be formulated into a linear programming problem. Some classical solutions for linear programming can be referred to elsewhere [9, 14]. Due to the computational complexities of linear programming, equivalent non-constrained problems such as the Basis Pursuit Denoising have been developed, which introduces the Lagrangian multiplier λ:

$$\text{BPDN: } \hat{x} = \text{argmin}_{x\in\mathbb{R}^N} \lambda\|x\|_{l1} + \frac{1}{2}\|y - \Phi x\|_{l2}^2, \tag{2.30}$$

where λ controls the recovery accuracy.

Some well-developed algorithms with higher convergence rates and less computational complexities have recently been developed for the solutions of the two problems in (2.29) and (2.30). Typical examples include Newton's stepping method [11], gradient projection [27], iterative shrinkage thresholding algorithms [19], Nesterov's method [6] and NESTA [7]. Links to more algorithms can be referred elsewhere [69]. Determination of the selection of appropriate algorithms for HDR measurement problems needs to be investigated.

2.6.2 Sparsifying transform and the design of measurement matrix

In practice, the source signal x is normally non-sparse. However, real world signals are naturally compressible in an appropriate Ψ -transform domain, *i.e.* they are normally sparse after a Fourier transform, cosine transform, wavelet transform, inner products with spline basis, or other transforms that involves the inner product with a sparsifying matrix. Here Ψ is a sparsifying transform which maps f to sparse coefficients x. Therefore, there are the sparse Ψ -domain coefficients x for a source signal f, *i.e.* $x = \Psi f$. If the transform matrix Ψ is orthonormal, $f = \Psi^T x$.

Given a $K \times N$ measurement matrix Φ and a sparsifying transform Ψ for the source signal f, an underdetermined system, the same as equation (2.27) can be constructed

$$y = \Phi f = Ux \text{ with } U = \Phi\Psi^T. \tag{2.31}$$

Section 2.6.1 introduced the uniform uncertainty property (UUP) for the synthetic measurement matrix U to guarantee an exact recovery. The question arises: how to design such a matrix with UUP? In most of cases, an appropriate design of the measurement matrix Φ is the central concern because Φ is directly involved in practical measurements. It is fortunate that there are the following simple example measurement matrices [10, 13] with which exact recovery can be achieved with high probabilities:

1. Gaussian measurements - random matrices with the entries complying with an independent identical Gaussian distribution.
2. Binary measurements. The entries of the $K \times N$ synthetic measurement matrix U are independently sampled from a Bernoulli distribution with $p = 1/2$.
3. Fourier measurements. U is obtained by selecting K rows uniformly at random from the $N \times N$ Fourier transform matrix.
4. Incoherent measurements. A typical example is obtained by selecting K rows uniformly at random from an $N \times N$ orthonormal matrix Ψ^T and renormalizing the columns. Let $\mu := \sqrt{N}\max_{i,j}\left|\langle\varphi_i, \psi_j\rangle\right|$ which is referred to as the mutual coherence between Φ and Ψ^T. The less coherence, the smaller amount of measurements needed.

Method 4 above, *i.e.* incoherent measurement, is applicable in many applications. The following simple example demonstrates the feasibility of the compressed sensing theorem with an incoherent measurement.

Assume a source signal $f \in R^N$ with the dimension N = 256 has S-sparse DCT (discrete cosine transform) random coefficients x where S = 8 (see the blue stemmed presentations in Figure 2-10a and b). Taking K = 40 random measurements (shown in red in Figure 2-10b), a Newton stepping inner point algorithm [11] is applied to iteratively recover x; the results in Figure 2-10c and d show that a high accuracy recovery can be achieved. This example clearly shows that with a sampling rate far smaller than the Nyquist rate, the source signal can still be recovered at a high level of fidelity.

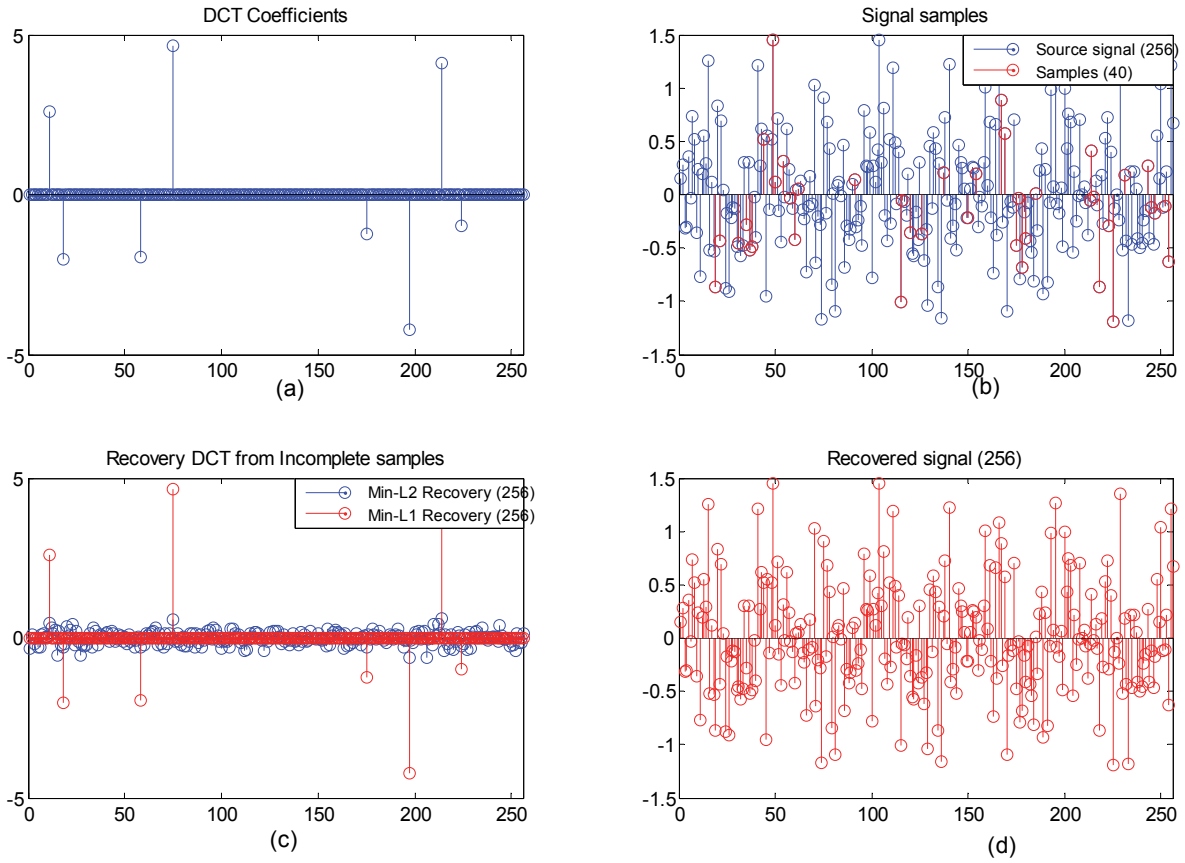

Figure 2-10. An exact sparse signal recovery with incomplete measurements. (a) shows the sparse DCT coefficients for the source signal. (b) presents the source signal (blue) and a set of 40 randomly selected samples (red). By applying the primal-dual inner point recovery reconstruction algorithm [11], (c) presents the first iteration result (blue) and the final recovery result (red). (d) shows the recovered source signal after an inverse DCT from (c).

More examples can be referred to in imaging processing [21, 70], where magnetic resonance imaging techniques have a number of applications. A simulation of the compressed sensing techniques in surface metrology was presented elsewhere [35]. Design of topography measurement instruments is different from the design of imaging devices. Regarding the instrumentation of the CS techniques in surface metrology, the following issues need in-depth research.

1. How to design optimal sampling schemes with low-rate incoherent measurements? For example, in which domain, such as the Euclidean space domain or Fourier domain, should the samples be collected? In which domain, or from which transform, should the source signal

have a sparse representation? Which inner product functions, such as a randomly centred impulse function or independent identically distribution Gaussian functions, should be used for collecting the samples? Are there advanced sampling methods that can increase the convergence rate in post iterative reconstruction?

2. How to design CS topography measuring instruments? For example, most current instruments acquire Euclidean space domain samples through a uniform sampling, which is obtained by the inner products with an impulse function. Since CS requires normally a random sampling to accelerate the sensing speed, how can the mechanics of the instrument be re-designed?

Overall, CS has shown its potential for extremely low rate sampling. Since the recovery accuracy is highly correlated with the number of samples, it can be postulated that high speed measurements can be achieved using the CS techniques if a small reconstruction error is acceptable. The lower sampling rate (lower than the Nyquist rate) characteristic of CS techniques is very useful in the detection of defects or other sparse features, in which cases accurate measurement is not strictly necessary.

2.7 SCANNING TECHNIQUES

Parallel sensing instruments with multiple sensors, for example a CCD array [42] or AFM tip array [53], do not require a dedicated design of the scan trajectories. For other single point-based instruments, for example stylus instruments and other scanning probe microscopes, sampling needs to be realised in a time sequence using appropriate scanning methods. A good scanning trajectory design can enhance the measuring speed and retain the sampling accuracy. A poor trajectory design has its measuring speed limited by the resonance frequency of the device.

The conventional "zig-zag" raster scan in a 2D plane normally requires a triangle waveform input for the fast axis (x-direction), and a slow staircase or ramp wave input for the slow axis (y-direction). Because the triangle wave has harmonics at odd positions on the full frequency domain, which attenuates at the rate of $1/n^2$, mechanical resonance can easily be excited when scanning in high speed. Hence, the current raster scan rate is limited to 10 to 100 times lower than the resonance frequency [18].

To achieve a faster scan rate, for example video rates over sixty frames per second, the working bandwidth of the motion system needs to be improved by introducing high-bandwidth feedback controllers [61]. Alternatively, the scan trajectory can be designed to minimise the frequency support of the driving signals, hence resonance of the scanner can be avoided. Table 2-3 shows recent developments of the design of scanning trajectories.

Among these methods, the Lissajous pattern scan has been highly recommended due to its single frequency input, *i.e.* the driven signals of x- and y-motion have very narrow frequency support.

Since advanced scanning methods, such as the Lissajous scan, Cycloid scan and spiral scan, do not exactly fit to a regular grid, a mapping from the non-grid scanning trajectories to regular grids is necessary. One of the most popular methods is the nearest point substitute based on Delaunay triangulation [72]. Stable and high-accuracy mapping algorithms also need investigation, for example Kriging [34].

Table 2-3. Advanced scanning strategies.

Scan patterns	Applications	Advantages	Disadvantages
Lissajous patterns	MRI, AFM [26, 39, 61]	• Extremely narrow frequency spectrum without exciting the resonance. • Low sensitivity to the measurement noise (generic and 1/*f* noise) for the feedback loop control. • Multi-resolution enabling fast preview.	• Requires higher vertical dynamic positioning accuracy for fast measurements.
Random scan	NA [39]	• Best immunization against noise impact.	• Difficult to implement due to mechanical limit.
Raster scan	Most of conventional and current applications in astronomy and microscopy	• Easily mapping to uniform sampling. • Even coverage for the field of view.	• Require acceleration at the turnarounds so only has stable positioning accuracy for the central area. • Strong directional sensitivity.
Billiard ball bouncing scan		• Even coverage for the field of view. • Immunization against directional noise and 1/*f* noise.	• Sharp turnarounds at the edge demanding stringent mechanical design.
Spiral scan	AFM [48, 49]	• Narrow frequency driving signal input has smooth dynamics without exciting the mechanical resonance.	• The constant linear velocity (CLV) mode results in a small circular artefact at the spiral centre. • The constant angular velocity (CAV) mode demands for higher vertical dynamic range for the edge area.
Cycloid scan	AFM[72]	• Single frequency input without exciting the resonance.	• Require larger area scan that is usually unwanted.
Sinusoidal scan	SNOM [33]	• Modification of raster scan fast axis triangle wave signal into sinusoidal wave to narrow the frequency support, hence resonance can be avoided.	• The non-smooth motion along the slow axis can be a drawback.

3 CONCLUSIONS

Statistically optimised sampling methods and approximation optimised sampling methods have been applied in coordinate metrology in recent years. Little development has been made for the measurement of HDR topographies, which require high speed measurements and large data manipulations.

The theorems of sampling for shift-invariant space signals are known not to be suitable for fast measurements because they require equivalent numbers of sample points to uniform sampling, though a small perturbation of the sampling positions is allowable.

Compressed sensing is a promising solution for the measurement of compressible signals, which includes many HDR topographies. However, the sparsifying transforms for different surface topographies need to be investigated and developed. Appropriate reconstruction algorithms will also be required. In addition to the mathematical issues, instrument designers need to conceive novel sensing methods for HDR topography measurement, for example sensing in the Fourier or other domains. Further questions regarding CS are: can adaptive sampling increase the reconstruction convergence rate? How can a random (Gaussian) sampling be quickly realised in the current instrument infrastructure?

The following future work is suggested:

1. Lissajous scan (or other advanced scan methods) integrated with intelligent sampling and/or stable reconstruction algorithms is a feasible direction for the development of fast measurement instruments under the current stylus instrument or scanning probe infrastructures.
2. Compressed sensing is a promising subject of research for HDR applications, but both theory and experimental work is required.

ACKNOWLEDGEMENT

This work was funded by the UK National Measurement System Engineering & Flow Metrology Programme, the FP7 project NANOMend, European Research Council (ERC-ADG-228117) and the UK's Engineering and Physical Sciences Research Council (EP/I033424/1).

REFERENCES

[1] Aldroubi A, Cabrelli C, Heil C, Kornelson K and Molter U 2010 Invariance of a shift-invariant space *J. Fourier Anal. Appl.* **16** 60-75

[2] Aldroubi A and Feichtinger H 1998 Exact iterative reconstruction algorithm for multivariate irregularly sampled functions in spline-like spaces: The L^p-theory *Proc. Amer. Math. Soc.* **126** 2677-86

[3] Aldroubi A and Gröchenig K 2001 Nonuniform sampling and reconstruction in shift-invariant spaces *SIAM Rev.* **43** 585-620

[4] Baraniuk R G 2007 Compressive sensing [lecture notes] *IEEE Signal Process. Mag.* **24** 118-21

[5] Barari A, ElMaraghy H A and Knopf G K 2007 Search-guided sampling to reduce uncertainty of minimum deviation zone estimation *J. Comput. Inf. Sci. Eng.* **7** 360-71

[6] Beck A and Teboulle M 2009 A fast iterative shrinkage-thresholding algorithm with application to wavelet-based image deblurring *Proc. IEEE ICASSP* p 693-6

[7] Becker S, Bobin J and Candès E 2011 NESTA: A fast and accurate first-order method for sparse recovery *SIAM J. Imaging Sci.* **4** 1-39

[8] Benedetto J and Ferreira P J S G 2001 *Modern sampling theory: mathematics and applications* (Birkhäuser)

[9] Boyd S and Vandenberghe L 2004 *Convex optimization* (Cambridge University Press)

[10] Candès E J 2006 Compressive sampling (Madrid, Spain) p 1433-52

[11] Candès E J and Romberg J 2005 L1-magic: recovery of sparse signals via convex programming. http:www.acm.caltech.edu/l1magic/

[12] Candes E J, Romberg J and Tao T 2006 Robust uncertainty principles: exact signal reconstruction from highly incomplete frequency information *IEEE T. Inform. Theory* **52** 489-509

[13] Candès E J, Romberg J K and Tao T 2006 Stable signal recovery from incomplete and inaccurate measurements *Commun. Pur. Appl. Math.* **59** 1207-23

[14] Chen S, Donoho D and Saunders M 1998 Atomic decomposition by basis pursuit *SIAM J. Sci. Comput.* **20** 33-61

[15] Cho M W and Kim K 1995 New inspection planning strategy for sculptured surfaces using coordinate measuring machine *Int. J. of Prod. Res.* **33** 427-44

[16] Claudiu L G and Richard K L 2013 Calibration of the scales of areal surface topography measuring instruments: part 3. Resolution *Meas. Sci. Technol.* **24** 105010

[17] Cox M G 1972 The numerical evaluation of b-splines *IMA J. Appl. Math.* **10** 134-49

[18] Croft D, Shedd G and Devasia S 2000 Creep, hysteresis, and vibration compensation for piezoactuators: atomic force microscopy application *Proc. Am. Control Conf.* p 2123-8

[19] Daubechies I, Defrise M and De Mol C 2004 An iterative thresholding algorithm for linear inverse problems with a sparsity constraint *Commun. Pur. Appl. Math.* **57** 1413-57

[20] Donoho D L 2006 Compressed sensing *IEEE T. Inform. Theory* **52** 1289-306

[21] Duarte M F, Davenport M A, Takhar D, Laska J N, Ting S, Kelly K F and Baraniuk R G 2008 Single-pixel imaging via compressive sampling *IEEE Signal Process. Mag.* **25** 83-91

[22] Duffin R J and Schaeffer A C 1952 A class of nonharmonic Fourier series *T. Am. Math. Soc.* **72** 341-66

[23] Edgeworth R and Wilhelm R G 1999 Adaptive sampling for coordinate metrology *Precis. Eng.* **23** 144-54

[24] Elkott D F, Elmaraghy H A and Elmaraghy W H 2002 Automatic sampling for CMM inspection planning of free-form surfaces *Int. J. Prod. Res.* **40** 2653 - 76
[25] Elkott D F and Veldhuis S C 2005 Isoparametric line sampling for the inspection planning of sculptured surfaces *Comput. Aided Design* **37** 189-200
[26] Feng H, Hong G, Silbersweig D, Stern E and Yihong Y 2003 Single-shot MR imaging using trapezoidal-gradient-based Lissajous trajectories *IEEE T. Med. Imaging* **22** 925-32
[27] Figueiredo M A T, Nowak R D and Wright S J 2007 Gradient projection for sparse reconstruction: application to compressed sensing and other inverse problems *IEEE J. Sel Top. Sign. Proces.* **1** 586-97
[28] Golub G H and Loan C F V 1996 *Matrix computations* (Johns Hopkins University Press)
[29] Grochenig K and Schwab H 2003 Fast local reconstruction methods for nonuniform sampling in shift-invariant spaces *SIAM J. Matrix. Anal. A.* **24** 899-913
[30] Halton J H 1960 On the efficiency of certain quasi-random sequences of points in evaluating multi-dimensional integrals *Numer. Math.* **2** 84-90
[31] Hammersley J M 1960 Monte Carlo methods for solving multivariable problems *Ann. NY Acad. Sci.* **86** 844-74
[32] Hu J, Li Y, Wang Y and Cai J 2004 Adaptive sampling method for laser measuring free-form surface *Int. J. Adv. Manuf. Tech.* **24** 886-90
[33] Humphris A D L, Hobbs J K and Miles M J 2003 Ultrahigh-speed scanning near-field optical microscopy capable of over 100 frames per second *Appl. Phys. Lett.* **83** 6-8
[34] Indek R, Tatjana K and Jörg S 2013 Application of ordinary kriging for interpolation of micro-structured technical surfaces *Meas. Sci. Technol.* **24** 095201
[35] Jianwei M 2010 Compressed Sensing for Surface Characterization and Metrology *IEEE T. Instrum. Meas.* **59** 1600-15
[36] Killmaier, T, Ramesh B and A 2003 Genetic approach for automatic detection of form deviations of geometrical features for effective measurement strategy *Precis. Eng.* **27** 370-81
[37] Kim W-S and Raman S 2000 On the selection of flatness measurement points in coordinate measuring machine inspection *Int. J. Mach. Tool. Manu.* **40** 427-43
[38] Kocis L and Whiten W J 1997 Computational investigations of low-discrepancy sequences *ACM T. Math. Software* **23** 266-94
[39] Kovacs A 2008 Scanning strategies for imaging arrays *Proc. SPIE* **7020**
[40] Ladislav K and William J W 1997 Computational investigations of low-discrepancy sequences *ACM T. Math. Software* **23** 266-94
[41] Leach R 2001 Measurement Good Practice Guide No. 37 The measurement of surface texture using stylus instruments(*Technical report, National Physical Laboratory,* UK)
[42] Leach R 2011 *Optical measurement of surface topography* (Springer)
[43] Leach R K, Jones C W, Sherlock B and Krysinski A 2013 The high dynamic range surface metrology challenge *28th ASPE Annual Meeting* p 149-52
[44] Lee G, Mou J and Shen Y 1997 Sampling strategy design for dimensional measurement of geometric features using coordinate measuring machine *Int. J. Mach. Tool. Manu.* **37** 917-34
[45] Li S Z 1995 Adaptive sampling and mesh generation *Comput. Aided Design* **27** 235-40
[46] Liu Y M and Walter G G 1995 Irregular sampling in wavelet subspaces *J. of Fourier Anal. Appl.* **2** 181-9
[47] Lustig M, Donoho D L, Santos J M and Pauly J M 2008 Compressed sensing MRI *IEEE Signal Process. Mag.* **25** 72-82
[48] Mahmood I A and Moheimani S O R 2009 Fast spiral-scan atomic force microscopy *Nanotechnology* **20** 365503
[49] Mahmood I A, Moheimani S O R and Bhikkaji B 2011 A new scanning method for fast atomic force microscopy *IEEE T. Nanotechnol.* **10** 203-16
[50] Parker J A, Kenyon R V and Troxel D E 1983 Comparison of interpolating methods for image resampling *IEEE T. Med. Imaging* **2** 31-9
[51] Petkovski M, Bogdanova S and Bogdanov M 2006 A simple adaptive sampling Algorithm *Proc. 14th Telecommunications forum* p 329-32

[52] Pharr M, Humphreys G and D G H 2004 *Physically based rendering: from theory to implementation* (Morgan Kaufmann)
[53] Rangelow I W, Ivanov T, Ivanova K, Volland B E, Grabiec P, Sarov Y, Persaud A, Gotszalk T, Zawierucha P, Zielony M, Dontzov D, Schmidt B, Zier M, Nikolov N, Kostic I, Engl W, Sulzbach T, Mielczarski J, Kolb S, Latimier D P, Pedreau R, Djakov V, Huq S E, Edinger K, Fortagne O, Almansa A and Blom H O 2007 Piezoresistive and self-actuated 128-cantilever arrays for nanotechnology applications *Microelectron. Eng.* **84** 1260-4
[54] Ratzel J N 1980 *The discrete representation of spatially continuous images* (PhD thesis, Massachusetts Institute of Technology)
[55] Roth R M and Seroussi G 1954 On irregularities of distribution *Mathematika* **1** 73-9
[56] Shannon C E 1949 Communication In The presence of noise *Proc. IRE* **37** 10-21
[57] Shih C S, Gerhardt L A, Chu W C-C, Lin C, Chang C-H, Wan C-H and Koong C-S 2008 Non-uniform surface sampling techniques for three-dimensional object inspection *Opt. Eng.* **47** 053606-15
[58] Slepian D 1976 On bandwidth *P. IEEE* **64** 292-300
[59] Tanaka H T 1995 Accuracy-based sampling and reconstruction with adaptive meshes for parallel hierarchical triangulation *Comput. Vis. Image Und.* **61** 335-50
[60] Terzopoulos D and Vasilescu M 1991 Sampling and reconstruction with adaptive meshes *IEEE Conf. CVPR.* p 70-5
[61] Tuma T, Lygeros J, Kartik V, Sebastian A and Pantazi A 2012 High-speed multiresolution scanning probe microscopy based on Lissajous scan trajectories *Nanotechnology* **23** 185501
[62] Van der Corput J G 1935 Verteilungsfunktionen i *Akad. Wetensch* **38** 813-21
[63] Walter G G 1992 A sampling theorem for wavelet subspaces *IEEE T. Inform. Theory* **38** 881-4
[64] Wang J 2012 *Sampling for the measurement of structured surfaces* (PhD thesis, University of Huddersfield, UK)
[65] Wang J, Jiang X, Blunt L A, Leach R K and Scott P J 2011 Efficiency of adaptive sampling in surface texture measurement for structured surfaces *Proc. 13th Intern. Conf. on Met. and Prop. of Eng. Surf.* 214-8
[66] Wang J, Jiang X, Blunt L A, Leach R K and Scott P J 2012 Intelligent sampling for the measurement of structured surfaces *Meas. Sci. Technol.* **23** 085006
[67] Whittaker J M 1928 The "Fourier" theory of the cardinal function *P. Edinburgh Math. Soc. (Series 2)* **1** 169-76
[68] Woo T C, Liang R, Hsieh C C and Lee N K 1995 Efficient sampling for surface measurements *J. Manuf. Syst.* **14** 345-54
[69] Yang A Y, Ganesh A, Zhou Z, Wagner A, Shia V, Sastry S and Ma Y 2013 Fast L1 minimization algorithms: homotopy and augmented Lagrangian method - implementation from fixed-point MPUs to many-core CPUs/GPUs.
[70] Yang A Y, Zihan Z, Balasubramanian A G, Sastry S S and Yi M 2013 Fast L1-minimization algorithms for robust face recognition *IEEE T. Image Proces.* **22** 3234-46
[71] Yao K 1967 Applications of reproducing kernel Hilbert spaces - bandlimited signal models *Inform. Control* **11** 429-44
[72] Yong Y K, Moheimani S O R and Petersen I R 2010 High-speed cycloid-scan atomic force microscopy *Nanotechnology* **21** 365503